3D Numerical Simulations of THz Generation by Two-Color Laser Filaments

Luc Bergé,[1] Stefan Skupin,[2,3] Christian Köhler,[1,2] Ihar Babushkin,[4] and Joachim Herrmann[5]

[1]*CEA-DAM, DIF, 91297 Arpajon, France*
[2]*Max Planck Institute for the Physics of Complex Systems, 01187 Dresden, Germany*
[3]*Institute of Condensed Matter Theory and Optics, Friedrich Schiller University, 07743 Jena, Germany*
[4]*Weierstrass-Institut für Angewandte Analysis und Stochastik, 10117 Berlin, Germany*
[5]*Max-Born-Institut für Nichtlineare Optik und Kurzzeitspektroskopie, 12489 Berlin, Germany*

Terahertz (THz) radiation produced by the filamentation of two-color pulses over long distances in argon is numerically investigated using a comprehensive model in full space-time-resolved geometry. We show that the dominant physical mechanism for THz generation in the filamentation regime at clamping intensity is based on quasi-dc plasma currents. The calculated THz spectra for different pump pulse energies and pulse durations are in agreement with previously reported experimental observations. For the same pulse parameters, near-infrared pump pulses at 2 μm are shown to generate a more than 1 order of magnitude greater THz yield than pumps centered at 800 nm.

For two decades, terahertz (THz) sources have attracted increasing interest for applications in noninvasive sensing, time-domain spectroscopy, medical sciences, environmental monitoring, security screening, and others [1]. Besides photoconductive switches or nonlinear crystals, an alternative generator consists of tightly focusing a laser pump and its second harmonic (SH) in noble gases or in air [2–6]. Such setups can deliver THz field amplitudes greater than 100 MV/m over spectral widths of 100 THz and more. At first, these findings were explained by optical rectification via third-order nonlinearity [2]. Later, a quasi-dc plasma current generated by the asymmetric two-color field [3,5] from the stepwise increase of the free electron density due to tunnel ionization [6,7] was proposed to be the key player.

On the other hand, ultrashort laser filaments covering long distances in loosely focused geometry can also be of interest in the production of THz radiation remotely. D'Amico *et al.* [8] first reported forward THz emission from one-color filaments propagating in air. THz yields can be even higher by 2 orders of magnitude when using two-color filaments [9–12]. Since the delivery of THz pulses in air is limited by diffraction and attenuation due to water vapor, THz generation in filaments is quite promising for remote sensing applications and the control of intense THz radiation at long distances [11,12]. In recent publications, the dependence of the THz yield on pump pulse energy and duration as well as on the dynamics of multiple filamentation was investigated experimentally [9,10]. In particular, increasing the pump pulse duration was shown to drastically increase the THz pulse energy [9].

Despite these previous results, there is still no clear understanding of the dominant physical mechanism for THz generation in two-color filamentation regime, namely, either rectification by four-wave mixing (FWM) or the plasma current generated by tunneling ionization. So far, theoretical studies have evaluated THz emission using simplified models [13,14], but no answer has been brought by comprehensive numerical modeling.

In the present Letter, we examine THz generation by two-color filamentation in argon by means of fully space-time-resolved three-dimensional (3D) numerical simulations. Computations of THz features are performed in single and multiple filamentation regimes, for different input pulse energies, durations, and pump central wavelengths, offering the unique possibility to get direct insight into the filament dynamics. Such simulations are very demanding as they involve strongly different scales, from the attosecond level necessary to resolve the ionization bunches to the picosecond one to extract the THz field, as well as from micrometer to meter for the spatial dimensions. Evaluating THz spectra computed from either Kerr or plasma current effects reveals that the latter are dominant during filamentation at clamping intensity, when self-focusing is balanced by the generated plasma. For 800 nm pump pulses with energies <10 mJ, our numerical results agree with experimental observations reporting a linear growth in the THz signal with respect to the pump peak power and an almost fourfold increase of the THz yield when doubling the pump pulse duration. Additionally, a 14 times greater THz energy is reported for pulses having the same beam parameters but operating at 2 μm wavelength instead of 800 nm. Near- and mid-IR pumps were recently proposed to achieve stronger THz fields [15] and waveform-controlled THz generation [16].

In our simulations, we use the unidirectional pulse propagation model [6,17] for linearly polarized pulses,

$$\partial_z \hat{E} = i\sqrt{k(\omega)^2 - k_x^2 - k_y^2}\,\hat{E} + i\frac{\mu_0 \omega^2}{2k(\omega)}\hat{\mathcal{P}}_{\text{NL}}, \quad (1)$$

where $\hat{E} = \hat{E}(k_x, k_y, z, \omega)$ denotes the Fourier transform, with respect to transverse coordinates and time, of the electric field. $k(\omega) = \omega n(\omega)/c$ is the wave number, c is the speed of light in vacuum, and $n(\omega)$ is the refractive index of argon [18]. The nonlinear polarization $\hat{\mathcal{P}}_{\mathrm{NL}} = \hat{P}_{\mathrm{Kerr}} + i\hat{J}_e/\omega + i\hat{J}_{\mathrm{loss}}/\omega$ originates from the Kerr effect ($P_{\mathrm{Kerr}} \propto n_2 E^3$) with nonlinear index $n_2 \simeq 10^{-19}$ cm^2/W, the electron current J_e, and a photon absorption term J_{loss}. $J_e(t)$ is governed by the plasma current equation $\partial_t J_e + J_e/\tau_e = q_e^2 E \rho_e/m_e$, where $\tau_e = 190$ fs is the electron collision time [7]; q_e, m_e, and ρ_e denote the charge, mass, and density of the free electrons created by tunnel ionization. All our filamentation patterns develop from intensities >25 TW/cm^2, for which a stepwise increase of the electron density at electric field maxima was already demonstrated [19]. We simulate the filamentation of pump pulses with 12% of their energy converted to the SH. The relative phase between fundamental and SH is chosen as $\pi/2$ at $z = 0$. The pump pulse has an initial amplitude profile $\sim \sqrt{P_{\mathrm{in}}/P_{\mathrm{cr}}} e^{-(x^{2N}+y^{2N})/w_0^{2N}-t^2/t_p^2}$ with pulse duration t_p, beam width w_0, and $N \geq 1$. Because of computational limitations, we restrict the propagation range to 50 cm. Spectral resolution was 1.25 THz; spatiotemporal steps were $\Delta x = \Delta y = 1.5$ μm and $\Delta t \simeq 0.05$ fs, for an adaptive step size in z decreasing to ~ 0.1 μm.

Figures 1(a) and 1(b) show the maximum intensity, peak electron density and THz yield of a single two-color filament created from an 800 nm, 270 μJ Gaussian pump pulse ($N = 1$) with $t_p = 20$ fs and $w_0 = 200$ μm, which corresponds to an input peak power $P_{\mathrm{in}} = 1.2 P_{\mathrm{cr}}$ [20]. This filament develops three focusing cycles along the propagation axis, associated with three bursts of plasma. Throughout the Letter, we compute the THz field and respective yield by applying a frequency window of $\nu \equiv \omega/2\pi < 80$ THz on the electric field and integrating

the resulting intensity distribution over the whole numerical box. The THz energy stays below ~ 60 nJ and shows an oscillatory behavior along the propagation axis. These oscillations, linked to the focusing cycles of the filament, occur because the generated THz field constantly leaves our numerical box. Figure 1(c) shows the single-cycled on-axis THz field, which reaches amplitudes up to 0.2 GV/m. Figure 1(d) details the first stages of the THz spectral broadening. Filament-induced THz spectra appear relatively flat, once the pump pulse has reached the clamping intensity. During propagation, the THz spectrum broadens until merging with the broadened pump spectrum. Two characteristic stages occur: At moderate pulse intensities <100 TW/cm^2 ($z \lesssim 4.5$ cm), the THz spectrum is depleted near zero frequencies, while for clamping intensity $\gtrsim 150$ TW/cm^2 ($z \gtrsim 5.7$ cm), the same spectrum increases in the region $\nu \to 0$.

To understand the previous observations, we now analyze the potential THz sources in Eq. (1) qualitatively:

On one hand, we insert the input field $E(t) = E_0\{\sqrt{1-r} e^{-t^2/t_p^2} \cos(\omega_0 t) + \sqrt{r} e^{-2t^2/t_p^2} \cos(2\omega_0 t + \theta)\}$ into the 1D version of Eq. (1), discarding transverse diffraction [21]. Here, r, ω_0, and θ denote the SH intensity fraction, the pump central frequency, and initial relative phase between the two colors, respectively. We let the pulse propagate to a certain distance for given input intensity $I \sim |E_0|^2$, and we compute the local THz yield ($\nu < 80$ THz), either from the Kerr nonlinearity (optical rectification by FWM) or from the plasma current (photocurrent mechanism), i.e.,

$$\hat{E}_{\mathrm{THz}}^{\mathrm{Kerr}} \propto \frac{\nu^2}{c^2} n_2 \widehat{E^3}, \qquad \hat{E}_{\mathrm{THz}}^{\mathrm{current}} \propto \mu_0 \widehat{\partial_t J_e}. \qquad (2)$$

For the above Gaussian two-color field, one has $\hat{E}_{\mathrm{THz}}^{\mathrm{Kerr}} \propto \nu^2 e^{-\pi^2 t_p^2 \nu^2/4}$, so that small spectral components $\nu \to 0$ are depleted, and we expect maximum growth at $\nu = 2/\pi t_p$. In
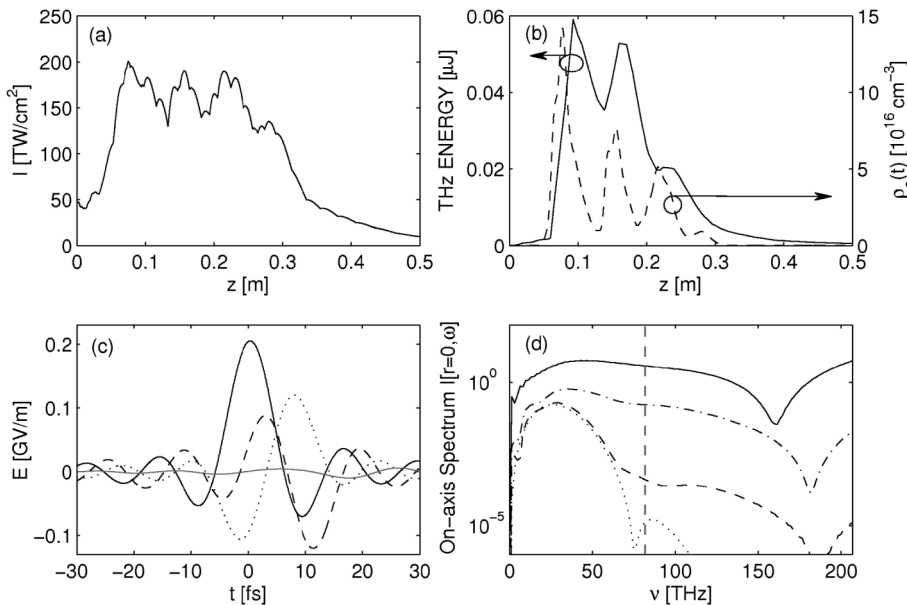

FIG. 1. (a) Peak intensity and (b) peak electron density (dashed curve) and THz yield (solid curve) for a single two-color filament in argon (800 nm pump, $t_p = 20$ fs, $w_0 = 200$ μm, $P_{\mathrm{in}} = 1.2 P_{\mathrm{cr}}$, $p = 1$ bar). (c) On-axis THz fields at $z = 8$ cm (dotted curve), $z = 9.3$ cm (solid curve), $z = 16$ cm (dashed curve), and $z = 0.3$ m (gray curve). (d) On-axis spectra at $z = 1$ cm (dotted curve), $z = 4.5$ cm (dashed curve), $z = 5.7$ cm (dash-dotted curve), and $z = 8$ cm (solid curve). The vertical gray dashed line indicates our THz window, $\nu < 80$ THz.
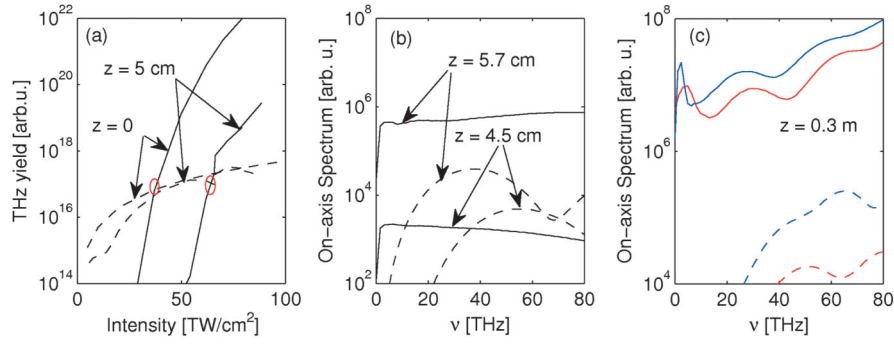
FIG. 2 (color).   (a) Local THz yield vs peak intensity evaluated from the 1D UPPE model (see text, $r = 0.12$, $\theta = \pi/4$, $t_p = 20$ fs).
Solid curves (dashed curves) show current-driven (Kerr-driven) THz yield. (b) Local spectra obtained from inserting 3D-propagated
on-axis pulse profiles of Fig. 1 into Eq. (2), using the previous plotstyles. (c) Same for the $30P_{cr}$ pulses addressed in Fig. 3 (red curves,
$t_p = 20$ fs; blue curves, $t_p = 40$ fs).

contrast, $\hat{E}_{THz}^{current} \propto \widehat{\rho_e E}$ [22] can generate near-zero fre-
quencies due to the stepwise increase of ρ_e in time [7].
On this basis, Fig. 2(a) displays the resulting local THz
yields, assuming a Kerr source (dashed curves) or a plasma
source (solid curves). For peak intensities >80 TW/cm^2,
the plasma-driven THz yield prevails over the Kerr-driven
yield by several orders of magnitude. Upon reaching 5 cm
long distances, the threshold intensity (red ellipses), above
which the plasma source dominates, becomes higher, which
we attribute to changes in the pulse shape, i.e., spectral
broadening of the pump.

On the other hand, we directly insert the on-axis propa-
gated electric field obtained from Eq. (1) at given distances

into the two expressions of Eq. (2). As a result, Fig. 2(b)
summarizes Kerr-driven and plasma-driven local THz spec-
tra computed from the 3D propagated fields at $z = 4.5$ cm
($I \simeq 94.5$ TW/cm^2) and $z = 5.7$ cm ($I \simeq 144$ TW/cm^2). As
expected, at moderate peak intensity <100 TW/cm^2, the
Kerr-driven THz generation dominates at higher frequen-
cies >40 THz. However, once intensity clamping occurs,
the photocurrent mechanism takes over.

Let us now investigate different pulse configurations with
larger peak power, $P_{in} = 30P_{cr}$, and a beam width of 1 mm
(Fig. 3). Using Eq. (1), we simulate a Gaussian pulse (red
curves), a slightly perturbed super-Gaussian pulse ($N = 2$)
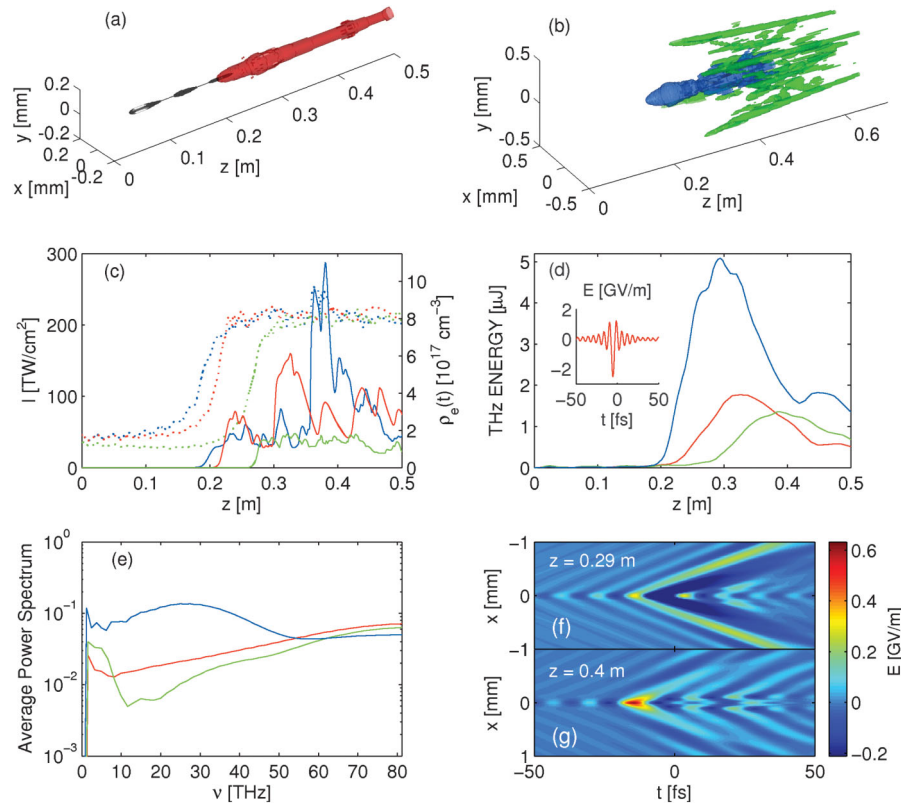(green curves) with $t_p = 20$ fs, and a Gaussian pulse with

FIG. 3 (color).   Two-color pulses with
$w_0 = 1$ mm, $P_{in} = 30P_{cr}$ at 800 nm. Red
curves: Gaussian pulse with $t_p = 20$ fs.
Green curves: super-Gaussian pulse with
$t_p = 20$ fs, initially perturbed by a 5%
amplitude random noise. Blue curves:
Gaussian pulse with $t_p = 40$ fs. [(a) and
(b)] Plasma channels (isoelectron-density
at $\rho_e = 2 \times 10^{16}$ cm^{-3}) with same color
coding. Black channel in (a) refers to the
single filament of Fig. 1. (c) Maximum
intensity (dotted curves, left axis) and
peak electron density (solid curves, right
axis). (d) THz yield for $\nu < 80$ THz.
Inset shows the on-axis THz field
achieved by the $30P_{cr}$, 20 fs Gaussian
pulse at $z = 0.46$ m. (e) Spatially inte-
grated power spectra at distances close to
maximum THz yield, i.e., $z = 0.3$ m
(blue), 0.35 m (red), and 0.4 m (green).
[(f) and (g)] THz field profiles in the (x, t)
plane ($y = 0$) for the 40 fs pulse at
(f) $z = 0.29$ m and (g) $z = 0.4$ m.

doubled duration $t_p = 40$ fs (blue curves). Figures 3(a) and 3(b) show the respective plasma channels. Compared to Fig. 1, the broader and more powerful beams self-focus later and produce longer filaments. The 20 fs Gaussian pulse with $30 P_{cr}$ (6.8 mJ pump energy) generates higher peak densities $\leq 6 \times 10^{17}$ cm^{-3} and does not decay into multiple filaments [Fig. 3(a)]. The plasma volume becomes greater with longer pulse durations, as the beam shape remains robust against modulational instability [Fig. 3(b)]. In contrast, using a noisy second-order super-Gaussian profile favors the emergence of multiple filaments [23]. These spread out the pulse energy inside the focal spot and lower the plasma response to some extent [Fig. 3(c)]. The THz yield reaches ~ 1.5 μJ for the 20 fs pulses [Fig. 3(d)]. With the results presented in Fig. 1, this value is consistent with the quasilinear growth of THz energy with the pump pulse energy reported in Ref. [9]. However, multiple filamentation prevents an optimal confinement of the plasma channel. In our example, between 4 and 8 optical filaments emerge, which indicates that the THz yield does not linearly increase with the number of filaments but instead with the input power of the pump pulse. As shown in the inset in Fig. 3(d), the THz field amplitude can reach 2 GV/m.

Having twice the pump energy, the 40 fs Gaussian pulse develops several temporal peaks and thus triggers more ionization events. The associated peak density can exceed 10^{18} cm^{-3} [Fig. 3(c)]. All these features have a direct impact on the THz generation and lead to an almost fourfold ($\times 3.6$) increase of the THz yield, achieving ~ 5.1 μJ ($\nu < 80$ THz) at $z \simeq 0.3$ m [Fig. 3(d)], compatible with Ref. [9]. In the much smaller frequency window $\nu < 5.5$ THz, we report a maximum THz yield of 350 nJ, in quantitative agreement with Ref. [10]. At $z = 0.3$ m, the on-axis electric field features a double-peaked temporal profile [24], which we insert into the two expressions of

Eq. (2) to identify the nonlinearity responsible for the THz signal growth. As shown by Fig. 2(c), also for this pulse configuration plasma currents clearly prevail over FWM contributions in the filament. Figure 3(e) displays spectra transversally integrated over the simulation box at distances close to respective maximum THz yield ($\nu < 80$ THz). These spectra exhibit components near zero frequency at intensity clamping, which again confirms that the photocurrent mechanism drives THz generation in this regime. Figures 3(f) and 3(g) finally evidence the large spatial extents of the THz fields due to diffraction.

Finally, we examine THz generation for near-infrared pump pulses. All laser parameters are kept unchanged compared with the pulse configuration discussed in Fig. 1, except the pump central wavelength taken as $\lambda_0 = 2$ μm. We adapt the gas pressure to $p = 6.44$ bar, in order to preserve the power content ($P_{in}/P_{cr} = 1.2$). From Ref. [7], local photocurrents are expected to increase their low frequency density for longer pump wavelengths, which also enhance the temporal asymmetry of the two-color field. Moreover, we expect a strong overlap with the pump spectrum directly contributing to THz emission. As shown by Fig. 4(a), self-focusing at 2 μm occurs earlier compared to that at 800 nm, owing to the reduction of the Rayleigh length, and the filament rapidly decays beyond 0.1 m. Plasma peaks attain 1.6×10^{18} cm^{-3}, mainly because of the increase of pressure. The THz yield is noticeably augmented to 0.8 μJ, i.e., close to 14 times the maximum THz energy supplied by a comparable 800 nm pump. The THz fields can attain amplitudes as high as 1.5 GV/m [see inset of Fig. 4(b)], i.e., of strength comparable to a 800 nm pump pulse with 30 critical powers (Fig. 3). Thus, near-infrared filaments, although self-channeling over shorter distances, can produce 1 order of magnitude higher THz fields than infrared pumps with same physical power.
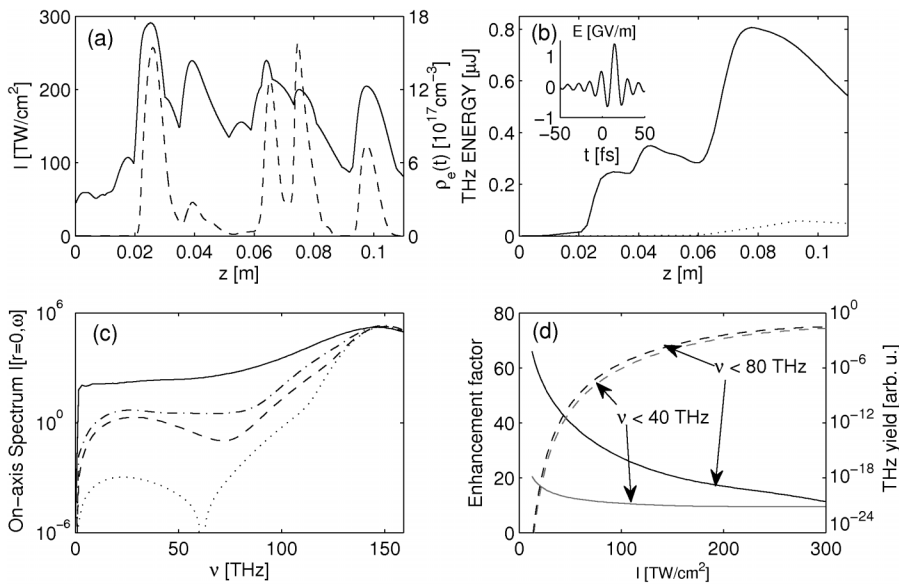

FIG. 4.   (a) Peak intensity (solid curve, left axis) and peak plasma density (dashed curve, right axis) of a two-color filament with a 2 μm pump pulse ($p = 6.44$ bar). (b) THz yield (solid curve). The dotted curve recalls Fig. 1(b) for a 800 nm pump. Inset shows the on-axis THz field at $z = 7$ cm. (c) On-axis spectra at $z = 1$ mm (dotted curve), 8 mm (dashed curve), 2 cm (dash-dotted curve), and 4 cm (solid curve). (d) Current-driven local THz yield (dashed lines, right axis) from 20 fs Gaussian pump pulses ($r = 0.12$, $\theta = \pi/4$, $p = 1$ bar) at 2 μm vs intensity for THz windows <40 THz (gray curves) and <80 THz (black curves). The solid lines (left axis) show the enhancement factors (ratios) of local THz yields over those from a pump at 800 nm with the same pulse configuration.

The THz spectrum merges from $z > 2$ cm with the pump bandwidth, so the THz yield computed in our reference window (< 80 THz) is partly caused by self-phase modulation of the pump pulse [Fig. 4(c)]. However, local THz yields computed from two-color Gaussian pulses using Eq. (2) show that the photocurrent mechanism clearly favors THz emission for longer pump wavelengths [Fig. 4(d)]. The same computations for the Kerr-driven local THz yield would show no enhancement at all.

In conclusion, 3D numerical simulations evidence the efficient generation of THz radiation over long distances by two-color laser filaments for various pump parameters. Local THz spectra evaluated from Kerr and plasma terms show that the photocurrent mechanism prevails in producing THz emission at clamping intensity in argon. We report a critical intensity of about 100 TW/cm^2, above which plasma currents dominate the Kerr nonlinearity for THz generation. However, we note that off-axis lower-intensity components of the filament may contribute additionally through FWM to the THz yield. Our results do emphasize the need of using field-dependent ionization rates to correctly describe THz emission in atmospheric multicolor filamentation. Experimental features are reproduced and justified, e.g., a larger peak power proportionally increases the THz yield, while the same yield is increased by a factor ~4 when doubling the pump pulse duration. Besides, pulses at 2 μm yield a tenfold THz energy compared to a 800 nm pump with same peak power. Importantly, we identify typical spectral signatures of Kerr-driven (low frequency depletion) and plasma-driven (low frequency build-up) THz generation. These signatures could be used as diagnostics in experiments to verify the origin of the THz emission.

[1] M. Tonouchi, Nat. Photonics **1**, 97 (2007).
[2] D. J. Cook and R. M. Hochstrasser, Opt. Lett. **25**, 1210 (2000).
[3] M. Kress, T. Löffler, S. Eden, M. Thomson, and H. G. Roskos, Opt. Lett. **29**, 1120 (2004).
[4] T. Bartel, P. Gaal, K. Reimann, M. Woerner, and T. Elsaesser, Opt. Lett. **30**, 2805 (2005).
[5] K. Y. Kim, A. J. Taylor, J. H. Glownia, and G. Rodriguez, Nat. Photonics **2**, 605 (2008).
[6] I. Babushkin, W. Kuehn, C. Köhler, S. Skupin, L. Bergé, K. Reimann, M. Woerner, J. Herrmann, and T. Elsaesser, Phys. Rev. Lett. **105**, 053903 (2010).
[7] I. Babushkin, S. Skupin, A. Husakou, C. Köhler, E. Cabrera-Granado, L. Bergé, and J. Herrmann, New J. Phys. **13**, 123029 (2011).
[8] C. D'Amico, A. Houard, M. Franco, B. Prade, A. Mysyrowicz, A. Couairon, and V. T. Tikhonchuk, Phys. Rev. Lett. **98**, 235002 (2007).
[9] T.-J. Wang, Y. Chen, C. Marceau, F. Théberge, M. Châteauneuf, J. Dubois, and S. L. Chin, Appl. Phys. Lett. **95**, 131108 (2009).
[10] T.-J. Wang, S. Yuan, Y. Chen, J.-F. Daigle, C. Marceau, F. Théberge, M. Châteauneuf, J. Dubois, and S. L. Chin, Appl. Phys. Lett. **97**, 111108 (2010).
[11] T.-J. Wang, J.-F. Daigle, S. Yuan, F. Théberge, M. Châteauneuf, J. Dubois, G. Roy, H. Zeng, and S. L. Chin, Phys. Rev. A **83**, 053801 (2011).
[12] J.-F. Daigle, F. Théberge, M. Henriksson, T.-J. Wang, S. Yuan, M. Châteauneuf, J. Dubois, M. Piché, and S. L. Chin, Opt. Express **20**, 6825 (2012).
[13] F. Théberge, M. Châteauneuf, G. Roy, P. Mathieu, and J. Dubois, Phys. Rev. A **81**, 033821 (2010).
[14] O. G. Kosareva et al., J. Infrared Millim. Terahz. Waves **32**, 1157 (2011).
[15] W.-M. Wang, S. Kawata, Z.-M. Sheng, Y.-T. Li, L.-M. Chen, L.-J. Qian, and J. Zhang, Opt. Lett. **36**, 2608 (2011).
[16] Y. Bai, L. Song, R. Xu, C. Li, P. Liu, Z. Zeng, Z. Zhang, H. Lu, R. Li, and Z. Xu, Phys. Rev. Lett. **108**, 255004 (2012).
[17] M. Kolesik and J. V. Moloney, Phys. Rev. E **70**, 036604 (2004).
[18] A. Dalgarno and A. E. Kingston, Proc. R. Soc. A **259**, 424 (1960).
[19] M. Uiberacker et al., Nature (London) **446**, 627 (2007).
[20] $P_{cr} \simeq 10.2$ GW is the critical power for self-focusing in argon at 800 nm.
[21] I. Babushkin, S. Skupin, and J. Herrmann, Opt. Express **18**, 9658 (2010).
[22] Here, we neglect the electron collision term for simplicity.
[23] L. Bergé, C. Gouédard, J. Schjødt-Eriksen, and H. Ward, Physica (Amsterdam) **176D**, 181 (2003).
[24] L. Bergé, S. Skupin, R. Nuter, J. Kasparian, and J. P. Wolf, Rep. Prog. Phys. **70**, 1633 (2007).